Editors' Suggestion

Perturbed Ion Temperature and Toroidal Flow Profile Measurements in Rotating Neoclassical Tearing Mode Magnetic Islands

L. Bardóczi,[1,2] A. Dudkovskaia,[3] R. J. La Haye,[1] J. D. Callen,[4] C. Chrystal,[1] and M. Podesta[5]
[1]General Atomics, Post Office Box 85608, San Diego, California 92186-5608, USA
[2]University of California, Irvine, California 92697, USA
[3]York Plasma Institute, School of Physics, Engineering and Technology, University of York, Heslington, York YO10 5DD, United Kingdom
[4]University of Wisconsin-Madison, Madison, Wisconsin 53706-1609, USA
[5]Princeton Plasma Physics Laboratory, Princeton, New Jersey 08543, USA

(Received 4 December 2023; accepted 16 January 2024; published 9 February 2024)

The perturbed ion temperature and toroidal flow were measured in rotating neoclassical tearing modes (NTM) in a tokamak for the first time. These toroidally and radially resolved profiles were obtained by impurity ion spectroscopy in a 2,1 NTM in DIII-D. In agreement with drift-kinetic simulations, the electron temperature profile is flat, while the ion temperature gradient is restored across the magnetic island O point in the presence of fast ions; the perturbed flow has minima in the O points and maxima at the X points. These measurements provide the first confirmation of the theoretically expected ion temperature and flow response to a magnetic island needed to predict the NTM onset threshold scaling for ITER and other future tokamaks.

DOI: 10.1103/PhysRevLett.132.065107

Introduction.—Magnetic reconnection is a fundamental phenomenon leading to field reconfiguration, plasma heating, jetting, and acceleration in space and astrophysical plasmas, such as magnetic storms in the Earth's magnetotail [1], flares and mass ejections in the solar corona [2], and formation of magnetic islands in laboratory plasmas [3,4]. Island structures are also common in atomic and molecular physics [5], solid state physics [6], laser science [7], nonlinear dynamics [8,9], and in interdisciplinary physics [10]. Neoclassical tearing modes (NTMs) are resistive magnetohydrodynamic (MHD) instabilities that form magnetic islands in high-performance thermonuclear fusion plasma experiments in tokamaks. The $m, n = 2, 1$ islands represent a major impediment in the development of operational scenarios for future fusion reactors, as they substantially decrease the energy and particle confinement and often lead to a violent and uncontrolled plasma termination, called a disruption [11,12] (m and n are the poloidal and toroidal mode numbers). NTMs are destabilized when MHD transients produce a seed island greater than the NTM threshold [13]. This threshold is set by the competition between stabilizing and destabilizing mechanisms, such as the bootstrap current perturbation [14] (j_{BS}) and the polarization current [15,16] (j_{pol}). These current perturbations arise from the combination of the electron and ion pressure gradient and flow response to the seed island [17]. Thus, understanding the plasma response to small magnetic islands is key for developing tearing stable operational solutions on present devices and extrapolating requirements to future reactors.

The local electron temperature perturbation ($\tilde{T}_{\mathrm{e}}$) is experimentally well constrained in magnetic islands [4,18,19], while the density is flat in the core of high-performance tokamak plasmas even in the absence of islands. Rotation averaged measurements have shown modification of the rotation profile in magnetic islands driven externally by resonant magnetic perturbations in tokamaks [20]. Also, the radial profile of the poloidal ion flow velocity [21] and turbulence perpendicular propagation [22] have been reported in static 1,1 and 3,2 islands in stellarators, respectively. However, the ion temperature ($\tilde{T}_{\mathrm{i}}$) and flow perturbations ($\tilde{v}_{\mathrm{i},\phi}$) induced by NTMs have not been measured in tokamak experiments before.

Overview.—We present simultaneous measurements of toroidally and radially resolved $\tilde{T}_{\mathrm{e}}$, $\tilde{T}_{\mathrm{i}}$, and $\tilde{v}_{\mathrm{i},\phi}$ profiles in NTM magnetic island chains. Both $\tilde{T}_{\mathrm{e}}$ and $\tilde{T}_{\mathrm{i}}$ have maxima near the island separatrices, while their phase jumps by π at the island center, as expected by theory [23]. Interestingly, while the electron temperature (T_{e}) profile is nearly flat at the O-point region, the ion temperature (T_{i}) profile is steep, in agreement with reduced drift-kinetic-NTM (RDK-NTM) modeling [17,24] predicting steep T_{i} at the O point resulting from a radial shift of drift-islands of co- and counterpassing ions. Further, $\tilde{v}_{\mathrm{i},\phi}$ has minima in the island O points and maxima at the X points suggesting that the ions inside the O point slow with the island. The flow phase is constant across the island, and jumps by π outside of the island separatrices. Inclusion of fast ions in the RDK-NTM modeling replicates this observation as well. These

measurements are particularly important, as they help constrain theoretical models predicting the NTM onset threshold scaling for the international thermonuclear experimental reactor (ITER) and beyond.

Experimental setup.—We studied magnetic islands in DIII-D advanced inductive plasmas whose relevant plasma parameters include major radius 1.78 m, minor radius 0.61 m, NBI (neutral beam injection) power up to $P_{\mathrm{NBI}} = 17$ MW (no electron cyclotron heating) [Fig. 1(a)], NBI torque up to $T_{\mathrm{NBI}} = 9$ Nm [Fig. 1(b)], toroidal magnetic field 2.04 T in the opposite direction of the plasma current, plasma current $I_{\mathrm{p}} = 0.78$ MA [Fig. 1(c)], normalized plasma beta $\beta_{\mathrm{N}} \approx 1.7$ [Fig. 1(c)], line averaged core density $n_{\mathrm{e}} = 3.15 \times 10^{19}$ m^{-3} (interferometry [25]) [Fig. 1(d)], $T_{\mathrm{e}} = 2.6$ keV [electron cyclotron emission [26] (ECE)] and ion temperature $T_{\mathrm{i}} = 2.6$ keV [charge exchange recombination [27] (CER)] at the $q = 2$ rational surface [Fig. 1(e)] (q is the safety factor).

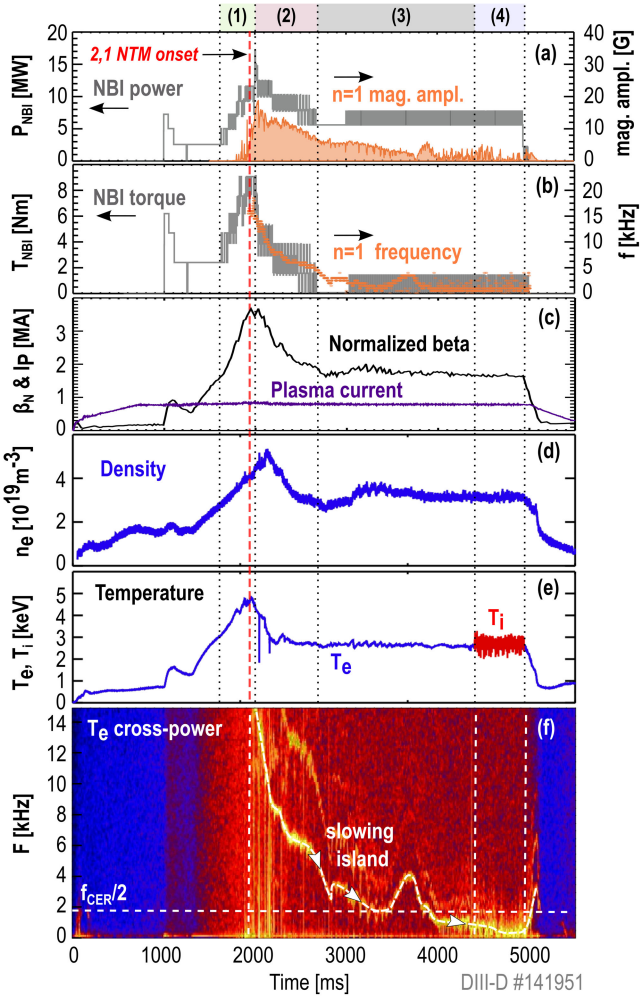

FIG. 1. (a) P_{NBI} and magnetic amplitude (A_1), (b) T_{NBI} and f_{i}. (c) β_{N} and I_{p}, (d) chord averaged electron density, (e) T_{e} and T_{i}, (f) cross power of T_{e} signals in the island region.

Diagnostics.—Magnetic islands are identified using the DIII-D electron cyclotron emission radiometer (ECE [26]) that provides T_{e} from measurements of optically thick, second harmonic (X-mode) electron cyclotron emission. T_{e} was probed at 12 radial locations within the island region with 480 kHz sampling rate, 0.3 cm above the tokamak midplane at the $\phi = 81°$ toroidal port. The island toroidal rotation allows probing T_{e} with respect to the helical phase (ξ) of the island ($\xi = m\theta - n\phi$, where θ and ϕ are the poloidal and toroidal angles). The ECE radial resolution is about 0.5 cm and the channels are separated by about 2 cm.

Magnetic characteristics, including the m and n mode numbers and the $n = 1$ magnetic root-mean-square amplitude (A_1) are determined using Mirnov-coil arrays [28].

$\tilde{T}_{\mathrm{i}}$ and $\tilde{v}_{\mathrm{i},\phi}$ are obtained by measurements of the Doppler broadening and Doppler shift of the carbon impurity charge exchange recombination spectroscopic line (CER [27]). The light collected by the CER optical system is produced by charge exchange between neutrals in the NBI and the carbon impurity ions. The measurement is spatially localized in the midplane at the point where the viewing chord crosses the NBI, at the $\phi \approx 20°$ toroidal angle. While this system can measure both the tangential and vertical components of the rotation, the tangential dominates due to poloidal flow damping at finite aspect ratio. This setup allows probing $\tilde{T}_{\mathrm{i}}$ and $\tilde{v}_{\mathrm{i},\phi}$ of the 2,1 islands at 7 radial locations with $\Delta r_{\mathrm{CER}} \approx 4$ cm radial separation. The shortest sampling interval of $\tilde{T}_{\mathrm{i}}$ and $\tilde{v}_{\mathrm{i},\phi}$ allowed by the CER hardware is 0.274 ms, giving a Nyquist frequency of $f_{\mathrm{CER}}/2 = 1.82$ kHz, and the data collection time window is limited to 540 ms at this high sampling rate. Thus, the measurement of $\tilde{T}_{\mathrm{i}}$ and $\tilde{v}_{\mathrm{i},\phi}$ calls for large islands rotating below $f_{\mathrm{CER}}/2$ within the preprogrammed CER data acquisition time window.

Experimental method.—Given that the island rotation brings the different phases of the island in view of the diagnostics, phase locking the ECE and CER data over many island cycles can be used to reconstruct the perturbed profiles, provided that $f_{\mathrm{i}} < f_{\mathrm{CER}}/2$ (island frequency). In addition, to obtain radial resolution, the full island width (W) must be larger than Δr_{CER}. These are challenging requirements, as most NTMs rotate typically with a few kHz or tens of kHz in DIII-D H-mode plasmas [29]. On the other hand, naturally slowing large islands quickly lock to the wall and disrupt the plasma, limiting the time available for collecting CER data. These effects prevent the reconstruction of $\tilde{T}_{\mathrm{i}}$ and $\tilde{v}_{\mathrm{i},\phi}$ via CER under typical plasma conditions in DIII-D.

To measure $\tilde{T}_{\mathrm{i}}$ and $\tilde{v}_{\mathrm{i},\phi}$, one must slow the NTM rotation and achieve torque balance at $f_{\mathrm{i}} < f_{\mathrm{CER}}/2$ with an island larger than Δr_{CER}. These conditions have been achieved in these experiments by using a NBI torque and power controller, leveraging that (i) NTMs are more likely to be destabilized as β_{N} is increased by raising P_{NBI}, (ii) the freely rotating NTM frequency naturally adjusts to the

plasma rotation, which can be controlled by T_{NBI}, and (iii) the wall electromagnetic drag arising from induced eddy currents can be reduced (to avoid locking and concomitant disruption) by shrinking the island width via reducing β_{N}. The cross-power spectrum of T_{e} signals in Fig. 1(f) shows the NTM onset and slow-down to about 700 Hz.

To reproducibly destabilize 2,1 NTMs in a series of repeat discharges, the plasma control system is programmed to ramp up P_{NBI} to increase β_{N} until a 2,1 island is destabilized and A_1 reaches 8 G. P_{NBI} and A_1 are shown in Fig. 1(a), β_{N} is shown in Fig. 1(c), this phase is labeled with (1) in Fig. 1. Next, P_{NBI} is reduced until β_{N} drops back to 1.7 to prevent the island growing to a large size and disrupting [phase (2)]. Along with this, T_{NBI} is dropped to slow the island rotation. These targets are maintained then until the plasma rotation at $q = 2$ and the $n = 1$ magnetic frequency decreases below 1 kHz [phase (3)]. The edge safety factor increases from an initial value of about 7.4 to about 8.4 as the plasma rotation slows, which moves the $q = 2$ surface slightly further from the wall, in favor of avoiding disruptions at slow rotation. Finally, a 540 ms long CER data acquisition takes place before the island locks to the wall [phase (4)]. This procedure is then repeated in a series of discharges to fine-tune the feedback algorithm until the slowly rotating island is sustained for a long enough time during the pre-programmed CER acquisition time window to collect sufficient data for reconstructing $\tilde{T}_{\mathrm{i}}$ and $\tilde{v}_{\mathrm{i},\phi}$.

Derivation of perturbed profiles.—The ECE and CER data are first transformed to the 2,1 island reference frame defined by the major radial coordinate R and helical angle $\xi = m\theta - n\phi$. The 2,1 island O point (X point) is at $\xi = 0$ ($\xi = \pi$) by definition. When the toroidal rotation is much faster than the poloidal rotation, then $\xi \approx \phi$ (for $n = 1$). To obtain the $\xi(t)$ coordinates of the $T_{\mathrm{e}}(R, t)$ measurements, first the times when the 2,1 island X point comes in view of the ECE diagnostic (t_i) were identified using that $\tilde{T}_{\mathrm{e}}$ has maxima at t_i inside of the $q < 2$ surface. To reduce noise, t_i are obtained from the principal mode singular value decomposition (SVD) signal calculated from three adjacent ECE channels. ξ is then linearly interpolated within each island cycle as $\xi_k = 2\pi(t_k - t_i)/(t_{i+1} - t_i)$, where $t_i \le t_k \le t_{i+1}$. Finally, $T_{\mathrm{e}}(R, \xi)$ is given by sorting $\tilde{T}_{\mathrm{e}}$ with respect to ξ_k in the full 540 ms measurement time window. Here, we assume that f_{i} is constant within one full toroidal turnover time (≈1.25 ms, but f_{i} can vary during the 540 ms acquisition window) and that W and the plasma conditions are stationary during the full analysis window. This analysis is then repeated for $\tilde{T}_{\mathrm{i}}$ and $\tilde{v}_{\mathrm{i},\phi}$ using the t_i (X-point times) derived previously from the ECE data. Given the high temporal resolution of the ECE system, this method gives robust mapping of the CER measurement times to ξ. Given the $\Delta\phi = 61°$ toroidal phase difference between the ECE and the CER probing locations, a phase difference of $\Delta\xi \approx \phi = 0.34\pi$ is expected between the ECE and CER data.

Electron temperature islands.—The contour plot of $T_{\mathrm{e}}(R, \xi)$ in the stationary phase [phase (4)] shows an island chain centered at $R_s \approx 194$ cm [Fig. 2(a)]. These islands encompass the $q = 2$ rational surface and are characterized by $n = 1$ mode number. Thus they are consistent with m, $n = 2$, 1 islands. The island magnetic flux contours are modeled by $\Omega(X, \xi) = 2X^2 + (\alpha X + 1)\cos(\xi)$, where $X = (R - R_s)/W$ and α is the radial asymmetry parameter [30]. Figure 2(a) shows that the T_{e} contours are close to the contours of Ω (solid black lines). In Fig. 2(a), the thick lines represent the island separatrices. W and α are determined by fitting the numerical solutions of the two-dimensional anisotropic heat transport model of magnetic islands [23] to T_{e} data by χ^2 minimization [18]. The full width of the island is about $W = 8$ cm. The radial profile intersecting the O point (X point) of the 2,1 island is flattened (steep) within the 2,1 island region [Fig. 2(d)]. The first Fourier harmonic amplitude of $\tilde{T}_{\mathrm{e}}$ [Fig. 2(g)] peaks near the separatrices of the island sets and the phase of the first Fourier harmonic ($\xi_{\mathrm{e},1}$) jumps by π near the island center, in agreement with theoretical expectation [23] and previous experiments [4,18].

Ion temperature islands.—The contours of $T_{\mathrm{i}}(R, \xi)$ show a clear island structure at the location of the 2,1 T_{e} island, with comparable radial width and the expected helical phase [Fig. 2(b)]. Interestingly, while $T_{\mathrm{e}}(R, \xi)$ is flat (steep) at the O point (X point) of the islands, T_{i} is just slightly flattened in the O point compared to the X point [Fig. 2(e)]. The radial profile of the first Fourier harmonic amplitude of the ion temperature peaks near the island separatrices [Fig. 2(e)]. The radial profile of the phase of $\tilde{T}_{\mathrm{i}}$ in Fig. 2(k) is consistent with π jump at the center of the island as in case of the $\tilde{T}_{\mathrm{e}}$ phase.

Perturbed toroidal rotation.—The contours of $\tilde{v}_{\mathrm{i},\phi}(R, \xi)$ in Fig. 2(c) show minima (maxima) at the island O points (X points). The radial profile of the first Fourier harmonic amplitude of the rotation ($\delta \mathrm{v}_{\phi,1}$) peaks near the island center where $\tilde{T}_{\mathrm{e}}$ and $\tilde{T}_{\mathrm{i}}$ exhibit a π phase jump. The phase of the first Fourier harmonic of the rotation ($\xi_{\mathrm{v},1}$) is flat across the island, while it jumps by π on the $R > R_s$ side of the island. As the island frequency (≈0.7 kHz) is slightly under the local plasma rotation frequency, slower thermal ion population in the O-point region is not surprising. The background rotation profile has significantly larger gradient closer the magnetic axis at $R < R_s$ compared to that at $R > R_s$ [Fig. 2(f)].

Reduced drift-kinetic simulations.—It is of interest to better understand the physics responsible for the measured properties of $\tilde{T}_{\mathrm{i}}$ and $\tilde{v}_{\mathrm{i},\phi}$. We utilize reduced drift-kinetic-NTM modeling based on the previously developed drift-island formalism [17,24,31], extended to capture the physics of fast ions. The numerical solution is provided by solving orbit-averaged drift-kinetic equations correct to

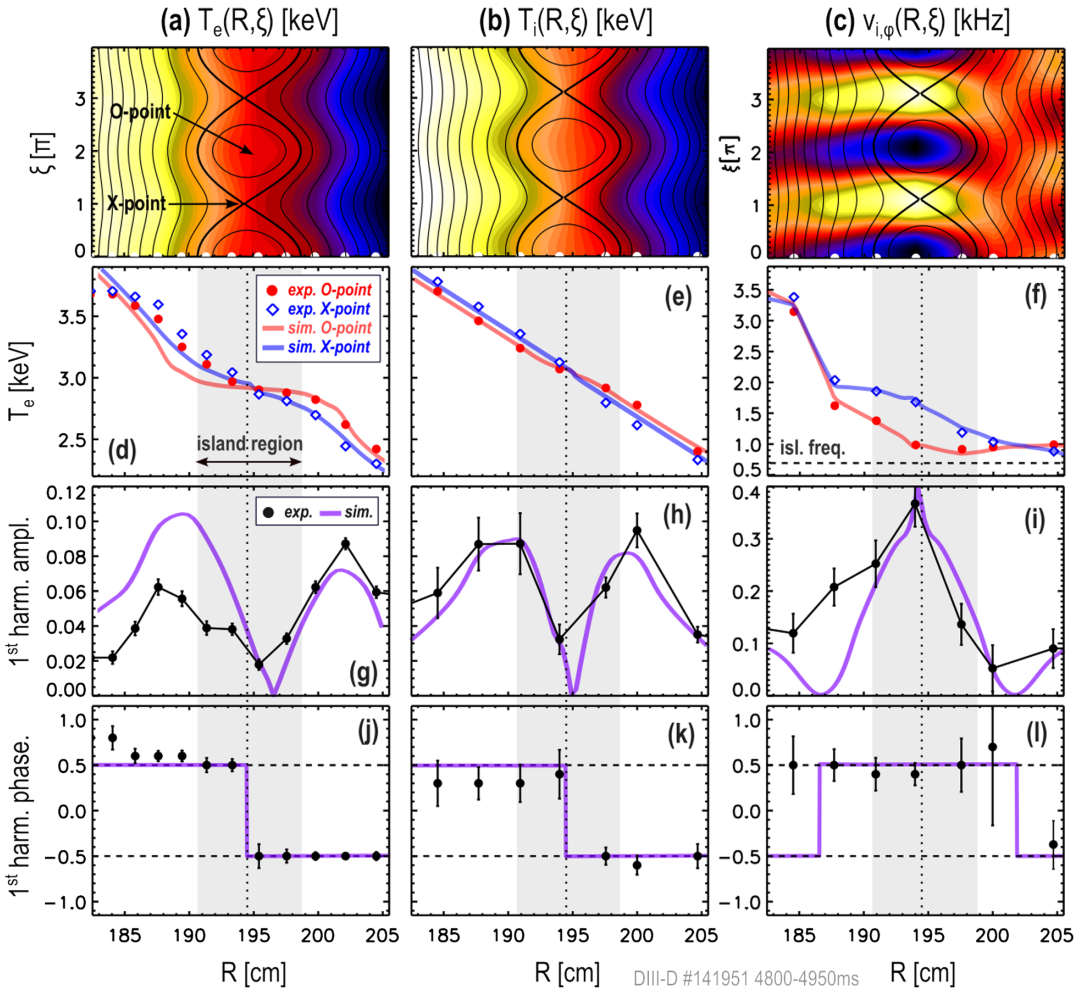

FIG. 2. Contours of (a) T_e, (b) T_i, and (c) v_i in the $R-\phi$ plane in DIII-D. Radial profiles of (d) T_e, (e) T_i, and (f) $\tilde{v}_{i,\phi}$ across the 2,1 island O point and X point. Radial profile of the 1st harmonic amplitude of (g) $\tilde{T}_e$, (h) $\tilde{T}_i$, and (i) $\tilde{v}_{i,\phi}$. Radial profile of the 1st harmonic phase of (j) $\tilde{T}_e$, (k) $\tilde{T}_i$, and (l) $\tilde{v}_{i,\phi}$. (d)–(l) include both DIII-D data (symbols) and results of RDK-NTM simulations (lines). Error bars in (d)–(f) are on the order of the symbol size.

second order in the Larmor radius over the system size expansion for a finite beta plasma. The bulk ion, electron, and fast ion distribution functions are coupled via plasma quasineutrality, which therefore ensures a self-consistent treatment of the electrostatic potential responsible for polarization effects on NTMs, and via collisions introduced through a simplified pitch angle scattering collision operator that conserves particles and momentum and allows for the slowing down effects [32,33].

The fast ion background information has been incorporated in RDK-NTM through the extended equilibrium ion distribution function, whose fast component is provided by TRANSP [34] and the thermal ion distribution is assumed to be Maxwellian. The effect of the island is not accounted for in TRANSP. The RDK-NTM solution accounts for the dissipation layer that surrounds the trapped-passing boundary in velocity space [13], as well as the layer around the magnetic island separatrix. Measured equilibrium and island parameters are provided as input. For simplicity, symmetric islands are assumed ($\alpha = 0$).

The drift-island formalism predicts that the passing particle distribution function is flattened across *drift* islands rather than the magnetic island [17,24,31]. These drift islands reproduce the magnetic island topology but have a radial shift by an amount proportional to the ion/electron poloidal Larmor radius, $\rho_{\theta,i/e}$, (i.e., Larmor radius evaluated with only the poloidal component of the magnetic field). This supports a contribution to the *ion* temperature gradient associated with passing ions, while the electron temperature gradient is still removed inside the island O point as $\rho_{\theta,e} \ll \rho_{\theta,i}$.

The simulation results overlayed in Fig. 2 with solid lines are generally in good agreement with the experimental data points. T_e is flat at the O point but steep at the X point while T_i is steep both at the O point and at the X point. The latter results from the ion drift islands that, being shifted radially with respect to the magnetic island (by an amount

comparable to the ion poloidal Larmor radius), were found to partially restore the ion temperature gradient across the magnetic island O point, even in the absence of fast ions. Inclusion of the fast ions enhances the drift-island radial shift, further steepening T_i. The amplitude of $\tilde{T}_e$ and $\tilde{T}_i$ peaks near the island separatrices, while the phase of $\tilde{T}_e$ and $\tilde{T}_i$ jumps by π at the island center, in agreement with the experiment. While drift kinetics accurately recovers the steepening of T_i, in close agreement with the experiment [Fig. 2(e)], it becomes less accurate for the electron component, in particular closer to the core region [Fig. 2(d)]. This could be caused by the radial profile of the equilibrium thermal diffusivity due to spatially nonuniform microinstability growth rates and/or due to the fact that the simulations employ radially symmetric islands while the islands are radially asymmetric in the experiment. To capture these effects one would require extensions to gyrokinetics and allow for the radial asymmetry in the magnetic island field perturbation.

The flow perturbation amplitude peaks in the island center [Fig. 2(i)], and jumps by π outside of the island approximately at $\pm 3W/2$ when the effect of the fast ions is included. This phase jump is in agreement with the experiment on the $R > R_s$ side of the island. The absence of this phase jump in the $R < R_s$ side of the island may be explained by the presence of a strong flow shear in that region in the experiment. In the absence of fast ions, the simulation shows a phase jump at the island separatrix. The flow O- and X-point profiles closely follow the experimental points in Fig. 2(f). Note that the ion parallel flow Fig. 2(f) is the sum of the perturbed piece localized in the island vicinity and the equilibrium component that contains global, neoclassical ion flows, that exist in the absence of the NTM. The first is calculated by RDK-NTM, while the latter contribution is provided by the experiment.

Summary.—We reported simultaneous measurements of toroidally and radially resolved $\tilde{T}_e$, $\tilde{T}_i$, and $\tilde{v}_{i,\phi}$ perturbation profiles of rotating neoclassical tearing mode magnetic islands in a tokamak. This was accomplished by slowing the rotation of 2,1 NTMs below the sampling rate of the charge exchange recombination spectroscopy diagnostic by using a neutral beam power and torque controller. These measurements show flat T_e at the O point and steep T_e at the X point, but steep T_i both at the O point and at the X point. Both $\tilde{T}_e$ and $\tilde{T}_i$ have maxima near the island separatrices and exhibit a π phase jump near the island center, approximately at the same location. $\tilde{v}_{i,\phi}$ has minima at the O points and maxima at the X points and the phase is constant within the islands but jumps by π outside of the islands. Within experimental uncertainties, the RDK-NTM simulations using experimentally measured equilibrium and island parameters are in agreement with the measurements. Inclusion of fast ions in the simulation is found to restore the T_i gradient across the magnetic island O point for medium magnetic island widths, arising due to the combined effect of the parallel streaming and magnetic drifts associated with fast, passing ions. Indeed, the passing ion distribution function was previously found to be flattened across drift islands rather than the actual magnetic island; and inclusion of fast ions then enhances the radial shift of these drift islands, steepening the total ion temperature profile across the magnetic island O point. This then reduces the bootstrap drive for NTMs, generating stabilizing flows inside the island. In addition, polarization currents are affected via the perturbed radial electric field around the island separatrix arising from the different electron and ion response and the broad flow perturbation. Thus, these measurements help constrain theoretical models of the NTM thresholds scaling for ITER and other next generation tokamaks.

This material is based upon work supported by the U.S. Department of Energy, Office of Science, Office of Fusion Energy Sciences, using the DIII-D National Fusion Facility, a DOE Office of Science user facility, under Awards No. DE-FC02-04ER54698 and No. DE-AC02-09CH11466. The data that support the findings of this study are available from the corresponding author upon reasonable request. The simulations in this work have been carried out within the framework of the EUROfusion Consortium, funded by the European Union via the Euratom Research and Training Programme (Grant Agreement No. 101052200—EUROfusion). This report was prepared as an account of work sponsored by an agency of the U.S. Government. Neither the U.S. Government nor any agency thereof, nor any of their employees, makes any warranty, express or implied, or assumes any legal liability or responsibility for the accuracy, completeness, or usefulness of any information, apparatus, product, or process disclosed, or represents that its use would not infringe privately owned rights. Reference herein to any specific commercial product, process, or service by trade name, trademark, manufacturer, or otherwise does not necessarily constitute or imply its endorsement, recommendation, or favoring by the U.S. Government or any agency thereof. The views and opinions of authors expressed herein do not necessarily state or reflect those of the U.S. Government or any agency thereof. Views and opinions expressed are however those of the author(s) only and do not necessarily reflect those of the European Union or the European Commission. Neither the European Union nor the European Commission can be held responsible for them.

[1] J. D. Huba and L. I. Rudakov, Hall magnetic reconnection rate, Phys. Rev. Lett. **93**, 175003 (2004).

[2] K. T. Osman, W. H. Matthaeus, J. T. Gosling, A. Greco, S. Servidio, B. Hnat, S. C. Chapman, and T. D. Phan, Magnetic

reconnection and intermittent turbulence in the solar wind, Phys. Rev. Lett. **112**, 215002 (2014).
[3] M. Yamada, Y. Ono, A. Hayakawa, M. Katsurai, and F. W. Perkins, Magnetic reconnection of plasma toroids with cohelicity and counterhelicity, Phys. Rev. Lett. **65**, 721 (1990).
[4] Z. Chang, J. D. Callen, E. D. Fredrickson, R. V. Budny, C. C. Hegna, K. M. McGuire, M. C. Zarnstorff, and T. group, Observation of nonlinear neoclassical pressure-gradient–driven tearing modes in TFTR, Phys. Rev. Lett. **74**, 4663 (1995).
[5] M. Conforti, A. Mussot, A. Kudlinski, S. R. Nodari, G. Dujardin, S. D. Biévre, A. Armaroli, and S. Trillo, Heteroclinic structure of parametric resonance in the nonlinear Schrödinger equation, Phys. Rev. Lett. **117**, 013901 (2016).
[6] Y. Lei and R. Fu, Heteroclinic chaos in a Josephson-junction system perturbed by dichotomous noise excitation, Europhys. Lett. **112**, 60005 (2016).
[7] M. Finardi, L. Flepp, J. Parisi, R. Holzner, R. Badii, and E. Brun, Topological and metric analysis of heteroclinic crisis in laser chaos, Phys. Rev. Lett. **68**, 2989 (1992).
[8] E. Stone, M. Gorman, M. el Hamdi, and K. A. Robbins, Identification of intermittent ordered patterns as heteroclinic connections, Phys. Rev. Lett. **76**, 2061 (1996).
[9] M. I. Rabinovich, R. Huerta, and P. Varona, Heteroclinic synchronization: Ultrasubharmonic locking, Phys. Rev. Lett. **96**, 014101 (2006).
[10] M. Rabinovich, A. Volkovskii, P. Lecanda, R. Huerta, H. D. I. Abarbanel, and G. Laurent, Dynamical encoding by networks of competing neuron groups: Winnerless competition, Phys. Rev. Lett. **87**, 068102 (2001).
[11] L. Bardóczi, T. L. Rhodes, T. A. Carter, A. B. Navarro, W. A. Peebles, F. Jenko, and G. McKee, Modulation of core turbulent density fluctuations by large-scale neoclassical tearing mode islands in the DIII-D tokamak, Phys. Rev. Lett. **116**, 215001 (2016).
[12] L. Bardóczi, L. C. Logan and E. J. Strait, Neoclassical tearing mode seeding by nonlinear three-wave interactions in tokamaks, Phys. Rev. Lett. **127**, 055002 (2021).
[13] H. R. Wilson, J. W. Connor, R. J. Hastie, and C. C. Hegna, Threshold for neoclassical magnetic islands in a low collision frequency tokamak, Phys. Plasmas **3**, 248 (1996).
[14] R. Carrera, R. D. Hazeltine, and M. Kotschenreuther, Island bootstrap current modification of the nonlinear dynamics of the tearing mode, Phys. Fluids **29**, 899 (1986).
[15] R. Fitzpatrick, F. L. Waelbroeck, and F. Militello, The influence of the ion polarization current on magnetic island stability in a tokamak plasma, Phys. Plasmas **13**, 122507 (2006).
[16] E. Poli, A. Bergmann, and A. G. Peeters, Role of kinetic effects on the polarization current around a magnetic island, Phys. Rev. Lett. **94**, 205001 (2005).
[17] K. Imada, H. Wilson, J. Connor, A. Dudkovskaia, and P. Hill, Finite ion orbit width effect on the neoclassical tearing mode threshold in a tokamak plasma, Nucl. Fusion **59**, 046016 (2019).
[18] L. Bardóczi, T. L. Rhodes, T. A. Carter, N. A. Crocker, W. A. Peebles, and B. A. Grierson, Non-perturbative measurement of cross-field thermal diffusivity reduction at the O-point of 2/1 neoclassical tearing mode islands in the DIII-D tokamak, Phys. Plasmas **23**, 052507 (2016).
[19] L. Bardóczi and T. E. Evans, Experimental observation of magnetic island heteroclinic bifurcation in tokamaks, Phys. Rev. Lett. **126**, 085003 (2021).
[20] K. Zhao, Y. Shi, S. H. P. Diamond, Y. S. 5, J. Cheng, H. Liu, N. Lie, Z. Chen, Y. Ding, Z. Chen, B. Rao, M. Leconte, J. Bak, Z. Cheng, L. Gao, X. Zhang, Z. Yang, N. Wang, L. Wang, W. Jin, L. Yan, J. Dong, G. Zhuang, and J-TEXT team, Plasma flows and fluctuations with magnetic islands in the edge plasmas of J-TEXT tokamak, Nucl. Fusion **55**, 073022 (2015).
[21] K. Ida, N. Ohyabu, T. Morisaki, Y. Nagayama, S. Inagaki, K. Itoh, Y. Liang, K. Narihara, A. Kostrioukov, B. J. Peterson, K. Tanaka, T. Tokuzawa, K. Kawahata, H. Suzuki, A. Komori, and L. E. Group, Observation of plasma flow at the magnetic island in the large helical device, Phys. Rev. Lett. **88**, 015002 (2002).
[22] T. Estrada, E. Ascasibar, E. Blanco, A. Cappa, C. Hidalgo, K. Ida, A. Lopez-Fraguas, and B. P. van Milligen, Plasma flow, turbulence and magnetic islands in TJ-II, Nucl. Fusion **56**, 026011 (2016).
[23] R. Fitzpatrick, Helical temperature perturbations associated with tearing modes in tokamak plasmas, Phys. Plasmas **2**, 825 (1995).
[24] A. V. Dudkovskaia, J. W. Connor, D. Dickinson, P. Hill, K. Imada, S. Leigh, and H. R. Wilson, Drift kinetic theory of neoclassical tearing modes in a low collisionality tokamak plasma: Magnetic island threshold physics, Plasma Phys. Controlled Fusion **63**, 054001 (2021).
[25] M. A. V. Zeeland, R. L. Boivin, T. N. Carlstrom, T. Deterly, and D. K. Finkenthal, Fiber optic two-color vibration compensated interferometer for plasma density measurements, Rev. Sci. Instrum. **77**, 10F325 (2006).
[26] M. E. Austin and J. Lohr, Electron cyclotron emission radiometer upgrade on the DIII-D tokamak, Rev. Sci. Instrum. **74**, 1457 (2003).
[27] K. H. Burrell, P. Gohil, R. J. Groebner, D. H. Kaplan, J. I. Robinson, and W. M. Solomon, Improved charge-coupled device detectors for high-speed, charge exchange spectroscopy studies on the DIII-D tokamak, Rev. Sci. Instrum. **75**, 3455 (2004).
[28] E. J. Strait, Magnetic diagnostic system of the DIII-D tokamak, Rev. Sci. Instrum. **77**, 023502 (2006).
[29] R. J. L. Haye, S. Gunter, D. A. Humphreys, J. Lohr, T. C. Luce, M. E. Maraschek, C. C. Petty, R. Prater, J. T. Scoville, and E. J. Strait, Control of neoclassical tearing modes in DIII-D, Phys. Plasmas **9**, 2051 (2002).
[30] J. A. Snape, K. J. Gibson, T. O'Gorman, N. C. Barratt, K. Imada, H. R. Wilson, G. J. Tallents, I. T. Chapman (the MAST team), The influence of finite radial transport on the structure and evolution of $m/n = 2/1$ neoclassical tearing modes on MAST, Plasma Phys. Controlled Fusion **54**, 085001 (2012).
[31] A. V. Dudkovskaia, L. Bardoczi, J. W. Connor, D. Dickinson, P. Hill, K. Imada, S. Leigh, N. Richner, T. Shi, and

H. R. Wilson, Drift kinetic theory of the NTM magnetic islands in a finite beta general geometry tokamak, Nucl. Fusion **63**, 016020 (2023).

[32] S. P. Hirshman, D. J. Sigmar, and J. F. Clarke, Neoclassical transport theory of a multispecies plasma in the low collision frequency regime, Phys. Fluids **19**, 656 (1976).

[33] S. Hirshman and D. Sigmar, Neoclassical transport of impurities in tokamak plasmas, Nucl. Fusion **21**, 1079 (1981).

[34] R. J. Hawryluk, *An Empirical Approach to Tokamak Transport* (Commission of the European Communities, Brussels, 1981), pp. 19–46.